TiC-MgO composite: an X-ray transparent and machinable heating element in a multi-anvil high pressure apparatus

Fang Xu, Longjian Xie, Akira Yoneda, Nicolas Guignot, Andrew King, Guillaume Morard, Daniele Antonangeli

▶ **To cite this version:**

Fang Xu, Longjian Xie, Akira Yoneda, Nicolas Guignot, Andrew King, et al.. TiC-MgO composite: an X-ray transparent and machinable heating element in a multi-anvil high pressure apparatus. High Pressure Research, In press, 10.1080/08957959.2020.1747452 . hal-02539501

HAL Id: hal-02539501
https://hal.science/hal-02539501v1

Submitted on 10 Apr 2020

HAL is a multi-disciplinary open access archive for the deposit and dissemination of scientific research documents, whether they are published or not. The documents may come from teaching and research institutions in France or abroad, or from public or private research centers.

L'archive ouverte pluridisciplinaire **HAL**, est destinée au dépôt et à la diffusion de documents scientifiques de niveau recherche, publiés ou non, émanant des établissements d'enseignement et de recherche français ou étrangers, des laboratoires publics ou privés.

TiC-MgO composite: An X-ray transparent and machinable heating element in a multi-anvil high pressure apparatus

Fang Xu[1], Longjian Xie[2*], Akira Yoneda[2], Nicolas Guignot[3], Andrew King[3], Guillaume Morard[1§], Daniele Antonangeli[1]

[1] Sorbonne Université, Muséum National d'Histoire Naturelle, UMR CNRS 7590, Institut de Minéralogie, de Physique des Matériaux et de Cosmochimie, IMPMC, 75005 Paris, France

[2] Institute for Planetary Materials, Okayama University, Misasa, Tottori 682-0193, Japan

[*] Currently at Bayerisches Geoinstitut, Universität Bayreuth, 95440 Bayreuth, Germany

[3] Synchrotron SOLEIL, L'Orme de Merisiers, Saint Aubin-BP48, 91192 Gif-sur-Yvette, France

[§] Currently at Institut des Sciences de la Terre (ISTerre), Université Grenoble-Alpes, 1381 rue de la scine F-38610 Gières

Abstract

TiC-MgO composite was developed as a heating element for X-ray study in the multi-anvil high pressure apparatus. We synthesized TiC-MgO blocks (50-70 wt.% of TiC) by compression in a cold isostatic press followed by baking in a gas flow furnace. Heaters of tubular shape were manufactured from the synthesized blocks either by lathe or numerically controlled milling machine from synthesized blocks. The so-produced heating elements have been proved to generate temperatures up to 2250 K at 10 GPa, condition where classical graphite heaters are not suitable anymore due to graphite-diamond transition. These new

heaters have been successfully used for *in situ* X-ray radiography and diffraction measurements on liquid Fe alloys, exploiting excellent X-ray transparency.

Key words: multi-anvil; heater; TiC-MgO composite; X-ray transparency; high temperature

1. Introduction

Pressure and temperature are fundamental thermodynamic variables that largely affect elastic, electronic, magnetic, structural and chemical properties of materials. Experiments under simultaneous high-pressure and high-temperature conditions are necessary to complement geophysical observations to reveal structures and properties of the Earth's deep interiors. Multi-anvil apparatus can compress large cell assembly with fine temperature control and reduced thermal gradients compared with diamond anvil cell, and over a significantly larger pressure and temperature range compared with Paris-Edinburgh press [1]. Last decades witnessed substantial technical developments in experimentation in multi-anvil apparatus, in particular in combination with the *in situ* X-ray observations, showing great versatility, with studies ranging from phase diagram and equation of state by X-ray diffraction (see review by [2]), to viscosity measurement by X-ray radiography [e.g. 3, 4], and density determination in liquids by X-ray absorption [e.g. 5, 6].

X-ray transparent heating elements are required to conduct *in situ* X-ray measurements in the multi-anvil apparatus at high temperature. Graphite is the most conventional heater for X-ray measurements under high pressures because of its high X-ray transparency. However, graphite heaters suffer malfunction at ~10 GPa because of transformation to diamond, which limits the use of such heaters over an extended pressure range. Metallic (Mo, Re and Ta) and lanthanum chromite ($LaCrO_3$) heaters are widely used as heating elements in high-pressure laboratory experiments. However, they are not suitable for *in situ* X-ray observations because of their low X-ray transparency. Recently, Xie et al. [7] developed boron-doped diamond (BDD) heater, which is very refractory and X-ray

transparent. However, owing to its hardness, it is hard to machine, making the production of tubular heaters out of BDD difficult. TiB_2 + BN composite (e.g. EBN grade from DENKA Ltd.) is widely used as a commercially available X-ray transparent heating element in high pressure experiments. However, the highest achievable temperature is limited to ~ 2000 K. In summary, there is a clear need to develop an alternative heater for *in situ* X-ray experiments at pressure and temperature exceeding 10 GPa and 2000 K.

Titanium carbide, TiC, is a highly refractory material having sodium chloride structure at ambient conditions [8]. The high melting point (3100 K at ambient pressure) [9], its low density (4.93 g/cm^3) and the absence of phase transformation up to 90 GPa [10], makes TiC a promising material for an X-ray transparent heating element. Taniguchi et al. [11] developed a TiC-diamond heater and successfully generated 2273 K at 10 GPa in a large-volume belt-type high pressure apparatus. In this study, TiC-diamond composite was synthesized by heat treatment of a mixture of diamond and non-stoichiometric TiC_{1-x} (x = 0.2) at ambient pressure. Recently, ~2073 K was achieved at ~10 GPa in a multi-anvil apparatus with (amorphous-)SiC/TiC composites [12]. However, none of the trials could provide a composite suitable to be machined in a tubular shape, which is the most reliable shape for heater in a multi-anvil high pressure cell. A commercial TiC-Al_2O_3 composite (NPA-2, Nippon Tungsten Co.,Ltd) has been applied for *in-situ* high pressure studies and a temperature of 2250 K was generated [13]. However, the hardness of NPA-2 makes the fabrication difficult, and thus the cost of a fabricated tubular heater very high.

In the present study, we report the protocol we used to synthesize TiC-MgO composite, which was proved to be easy to machine in tubular heaters used to generate high

temperature under high pressure in a multi-anvil apparatus. The TiC-MgO heaters exhibited not only stable ultra-high temperature generation, but also a good X-ray transparency, as tested during *in situ* radiography and diffraction measurements of liquid Fe-S alloys performed at synchrotron SOLEIL.

2. Experiments

A. Synthesis of TiC-MgO blocks

TiC-MgO starting material was prepared by mixing of TiC and MgO powders with different TiC concentrations, i.e. 50 and 70 wt.% (hereafter, we refer it as TiC-50 and TiC-70, respectively), in an agate mortar with either ethanol or acetone. We substituted 15wt.% of MgO by $Mg(OH)_2$ to enhance quality of sintering. The obtained TiC-MgO-$Mg(OH)_2$ mixtures were dried at 80°C in vacuum to remove remnant acetone/ethanol before molding. The mixtures were compressed at 200 MPa for 5 minutes in a cold isostatic press (CIP) and then calcinated in a gas flow furnace under reducing atmosphere of Ar+10% H_2 at 1273 K for 2-5 hours with a rising rate of 2 K/min. Fig.1a shows rods recovered after calcination process.

The TiC-MgO blocks were machined by lathe or numerically controlled (NC) milling machine into tube shaped heaters of desired dimensions (Figure 1b). Through the machining processes, it was observed that the machinability improves with increasing MgO content in the blocks. Further thinning is mechanically possible, while not necessary for our purpose of practical heaters for stable temperature generation in high pressure experiment.

Microstructure of recovered TiC-MgO blocks observed by a field emission scanning electron microscope (SEM-FEG) (Zeiss Ultra55) at IMPMC, Sorbonne University, France,

is illustrated in Fig.2. Sintered TiC-MgO blocks consist of TiC grains with ~1-4 μm size and finer grains of MgO. MgO grains distribute homogeneously in the TiC matrix, while some small clusters can be seen both in TiC-70 and TiC-50. X-Ray powder diffraction measurements were carried out at the X-ray diffraction platform of the IMPMC on a Rigaku MM007HF diffractometer for phase identification. Diffraction patterns of the TiC-MgO show no obvious brucite ($Mg(OH)_2$) peaks (Fig. 3), which indicates a complete dehydration during annealing. No peaks of TiO (partial reduction of MgO by TiC) [14], TiO_2 (oxidization of TiC), $MgTi_2O_5$, $MgTiO_3$ and Mg_2TiO_4 resulting from TiO_2-MgO reaction [15] were observed in the diffraction pattern. A small amount of Ti and $TiC_{0.5}H_{0.707}$ might be present in the bulk material (Fig. 3), as results of the reducing sintering atmosphere provided by Ar+10% H_2 [16, 17].

B. Tests of heating performances

We tested heating performance of the sintered TiC-MgO heater by carrying out high pressure and high temperature experiments in the Kawai-type multi-anvil apparatus installed at Institute for Planetary Materials, Okayama University, Japan. Fig. 4a and Fig. 4b show schematic view of the cell assemblies. Pressure of 10 GPa was generated using WC cubes with a 4 mm truncated edge length. Table 1 summarizes experimental specifications including one run for which TiC-Al_2O_3 (50 wt.%) composite heater (obtained following the same sintering procedure with TiC-MgO composite) was used as a possible alternative for TiC-MgO composite.

C. Application to in situ study on liquid Fe alloys

In situ radiography and diffraction experiments were conducted in the DIA-type multi-anvil apparatus installed at beamline PSICHE, SOLEIL, France. Fig. 4c shows the cell assembly used in these experiments. Boron-15 wt.% MgO composite (Xie et al., under review) was used both for pressure medium and gaskets in order to minimize the X-ray absorption of the sample environment. Pressure was generated by WC cubes with a 4 mm truncated edge length and determined through the equation of state of MgO marker placed at the thermocouple junction. The Fe-FeS powder mixture starting material was loaded in a sapphire capsule with caps made of BN.

After having reached the target load, heating was performed with voltage control. X-ray shadowgraphs of cell assembly were collected on a fluorescence screen and detected by a high-speed CCD camera (C9300, Hamamatsu Co., Japan). Energy dispersive diffraction patterns were collected on a germanium solid-state detector for increasing temperature (typical temperature step size 100 K). Upon complete melting, assessed by appearance of a diffuse scattering signal and disappearance of diffraction peak, energy-dispersive diffraction patterns were collected in a 2θ angle range from 2.5 to 25°, with a step size of 0.2° by using a germanium solid-state detector. Such combined angle- and energy-dispersive structural analysis and refinement (CAESAR) method allows recording the diffuse scattering signal from the liquid sample over a large reciprocal space (Q) range [18].

3. Result and discussion

A. Results of the heating performance tests

Fig. 5a shows the power-temperature relationships recorded during the test heating runs employing TiC-Al_2O_3 and TiC-MgO heaters, while Fig. 5b shows their Arrhenius plots of electrical conductivity. Run with TiC-Al_2O_3 composite heater was well performed up to 1970 K, temperature above which the thermocouple started having an anomalous reading. We ascribed this malfunctioning to the melting of the heater, as confirmed by inspection of the recovered cell (Fig. 6a). As this melting temperature is lower than the temperature achieved using NPA-2 in [13], the observed melting might have been caused by minor impurities associated to the sintering process. As for runs with TiC-MgO composites, temperature is very stable (±2 K) till the highest temperature reached in each run. No obvious melting was observed in the images of the recovered cells (Fig. 6b, c, d). The higher heating efficiency of runs 1K2881 and 1K2890 is a direct consequence of the lower thermal conductivity of the boron-15 wt.% MgO pressure medium used in these two runs (Fig. 2a), with respect to conventional MgO-5 wt.% Cr_2O_3 pressure medium used in the other runs (Xie et al., under review).

In both test runs of 1K2892 and 1K2894, for which we used the same cell assembly (Fig. 4b), we successfully generated high temperatures above 2100 K. Obviously, TiC-70 has higher electrical conductivity than TiC-50 due to the higher content of conductive TiC. During heating, the electrical conductivity of the TiC-MgO heaters increased until ~ 700 K mainly as an outcome of the compaction process (i.e. improvement of contact between heating elements and electrodes by deformation of materials). Then, we observed the

opposite trend, with conductivity decreasing with increasing temperature, which we attribute to the metal-like electric conduction of TiC. On the contrary, the TiC-Al_2O_3 heater (1K2881) showed continuous increase of electrical conductivity, possibly due to the high strength of corundum and limited plastic deformation under high temperature. Both heating of 1K2892 and 1K2894 was intentionally terminated when we started observing an increase of heater resistance accompanied by a decrease of temperature (Fig.5a). No temperature instability was recorded until then. No obvious signature of heater melting was found in the SEM image of recovered assembly (Fig.6b, c, d). Since our heater may contain a small amount of Ti-C-H phases, whose melting temperature, close to that of metallic Ti (~2000 K), is much lower than that of TiC, we could ascribe the failure of heater to the melting of these minor phases.

In summary, both TiC-70 and TiC-50 were proved to be suitable heaters, capable of generating temperatures exceeding 2000 K in multi-anvil apparatus. Given the similar heating performance, TiC-50 heater is more recommended because of its higher machinability. Furthermore, its lower electric conductivity allows making thicker tubular heaters, enhancing mechanical strength of heating elements.

As the resistivity of TiC-MgO heaters is comparable to that of graphite heaters, conventional power supply system can be used, without requiring any modification.

B. Results of applications to in situ study on liquid Fe alloys

The X-ray transparency of TiC-MgO heaters was compared with that of classic graphite heaters by using the same cell assembly. It is well known that graphite has the highest X-ray transparency among the available heaters used for experimentation in large volume press, due to the small atomic number of carbon. As shown in Fig. 7, radiographies of Fe-S sample

surrounded by TiC-MgO heater are as clear as those obtained using graphite heater. Sharp contrast among materials in the cell is very beneficial for quick identification of sample position and geometry.

Thanks to the use of TiC-MgO heaters we collected good quality CAESAR scans, with high signal to noise ratio, over a pressure and temperature range inaccessible with graphite heaters (Table 1 and Fig. 8). Data obtained using TiC-MgO heaters and using graphite heaters are overall comparable, with intensity in the case of TiC-MgO only slightly lower than for graphite heater. The high quality diffraction data over a large energy and angular range enable to obtain accurate structure factor over a large range of Q. Concerning stability and endurance as a furnace, the TiC-MgO composite heater stably operated at 10 GPa for more than 9 hours, at temperatures ranging from 1215 to 2145 K, with stable temperature maintained for about 1 hour for each temperature step (100 K increment) (MA41), granting enough time for thorough investigation and data collections.

Acknowledgment

We would like to thank B. Baptiste for his help with XRD measurements. The synchrotron radiation experiments were performed under SOLEIL proposals 20170506, 20171307 and 20181797. This project has received funding from the European Research Council (ERC) under the European Union's Horizon 2020 research and innovation program (Grant agreement No. 724690).

Reference

[1] Ito, E., 2007. 2.08 Theory and practice-multianvil cells and high-pressure experimental method. Mineral physics. In: Treatise on Geophysics, vol. 2, pp. 197-230.

[2] Katsura, T., 2007. Phase-relation studies of mantle minerals by in situ X-ray diffraction using multianvil apparatus. In: Advances in High-Pressure Mineralogy: Special Papers-geological society of America, 421, pp.189.

[3] Kanzaki M., Kurita K., Fujii T., Kato T., Shimomura O., Akimoto S., 1987. A new technique to measure the viscosity and density of silicate melts at high pressure. In: Geophysics Monograph 39: High-Pressure Research in Mineral Physics, pp. 195-200.

[4] Xie, L., Yoneda, A., Yamazaki, D., Manthilake, G., Higo, Y., Tange, Y., Guignot, N., King, A., Scheel, M., Andrault, D., 2020. Formation of bridgmanite-enriched layer at the top lower-mantle during magma ocean solidification. Nature Comm. 11(1), pp.1-10.

[5] Sanloup, C., Guyot, F., Gillet, P., Fiquet, G., Mezouar, M., Martinez, I., 2000. Density measurements of liquid Fe-S alloys at high-pressure. Geophys. Res. Lett., 27, pp.811-814.

[6] Sakamaki, T., Ohtani, E., Urakawa, S., Suzuki, A., Katayama, Y., 2009. Measurement of hydrous peridotite magma density at high pressure using the X-ray absorption method. Earth Planet. Sci. Lett., 287, pp.293-297.

[7] Xie, L., Yoneda, A., Yoshino, T., Yamazaki, D., Tsujino, N., Higo, Y., Tange, Y., Irifune, T., Shimei, T., Ito, E., 2017. Synthesis of boron-doped diamond and its application as a heating material in a multi-anvil high-pressure apparatus. Rev. Sci. Inst., 88, p.093904.

[8] Chang, R., Graham, L.J., 1966. Low-temperature elastic properties of ZrC and TiC. J. Appl. Phys., 37, pp.3778-3783.

[9] Sokolov, P. S., Mukhanov, V. A., Chauveau, T., Solozhenko, V. L., 2012. On melting of silicon carbide under pressure. J. Superhard Materials, 34(5), pp.339-341.

[10] Yoshida M, Onodera A., 1993. Pressure-induced phase transition in SiC. Phys. Rev. B Condens. Matter., 48, pp.10587-10590.

[11] Taniguchi, T., Akaishi, M., Kanke, Y., Yamaoka, S., 2004. TiC-diamond composite disk-heater cell assembly to generate temperature of 2000 ℃ in a large-volume belt-type high-pressure apparatus at 10 GPa. Rev. Sci. Inst., 75(6), pp.1959-1962.

[12] Guan, L., Schwarz, M., Zhang, R., Kroke, E., 2016. Polymer-precursor-derived (am-) SiC/TiC composites for resistive heaters in large volume multi-anvil high pressure/high-temperature apparatus. High Press. Res., 36(2), pp.167-186.

[13] Terasaki, H., Rivoldini, A., Shimoyama, Y., Nishida, K., Urakawa, S., Maki, M., Kurokawa, F., Takubo, Y., Shibazaki, Y., Sakamaki, T., Machida, A., 2019. Pressure and composition effects on sound velocity and density of core-forming liquids: implication to core compositions of terrestrial planets. J. Geophys. Res.: Planets, 124(8), pp.2272-2293.

[14] Ueltz, H.F.G., 1950. Sintering reactions in MgO-TiC mixtures. J. Amer. Ceram. Soc., 33, pp.340-344.

[15] Wechsler, B.A., Navrotsky, A., 1984. Thermodynamics and structural chemistry of compounds in the system MgO-TiO_2. J. Solid State Chem., *55*(2), pp.165-180.

[16] Fedorov, L.Y., Karpov, I.V., Ushakov, A.V., Lepeshev, A.A., 2015. Influence of pressure and hydrocarbons on carbide formation in the plasma synthesis of TiC nanoparticles. Inorganic Materials, 51(1), pp.25-28.

[17] Renaudin, G., Yvon, K., Dolukhanyan, S.K., Aghajanyan, N.N., Shekhtman, V.S., 2003. Crystal structures and thermal properties of titanium carbo-deuterides as prepared by combustion synthesis. J. Alloys Compounds, 356, pp.120-127.

[18] Wang, Y., Uchida, T., Von Dreele, R., Rivers, M.L., Nishiyama, N., Funakoshi, K.I., Nozawa, A., Kaneko, H., 2004. A new technique for angle-dispersive powder diffraction using an energy-dispersive setup and synchrotron radiation. J. App. Crystal., 37, pp.947-956.

Figure captions

Fig.1 Pictures of synthesized TiC-MgO blocks (a) and machined tubes (b). The color difference in (b) is due to the low/high TiC (50/70 wt.%) concentration. We successfully obtained tube shape heaters of 3.5-5.0 mm length with OD/ID of 2.0-2.4/1.6 mm and 2.4/1.8 (OD: outer diameter, ID: inner diameter).

Fig.2 Electron back scattered images of sintered rods of TiC-70 (a, b) and TiC-50 (c, d). Bright and dark grains correspond to TiC and MgO, respectively.

Fig. 3 X-ray diffraction patterns of the sintered TiC-MgO. Monochromatic light from a rotating Mo anode ($\lambda K\alpha 1$ = 0.709319 Å) was used. The systematically observed second peaks marked by vertical sticks are diffraction peaks from $K\alpha 2$ emission ($\lambda K\alpha 2$ = 0.713609 Å). No obvious shift of TiC or MgO peaks was observed, suggesting no chemical reaction or inter-grain diffusion. The black arrows marked the indexed peaks of $TiC_{0.5}H_{0.707}$, by assuming same peak positions between $TiC_{0.5}H_{0.707}$ and $TiC_{0.5}D_{0.707}$.

Fig. 4 Cell assemblies used for high pressure heater test experiments with boron-MgO (boron-15 wt.% MgO) (a, c) and MgO-Cr_2O_3 (MgO-5 wt.% Cr_2O_3) (b) as pressure medium. Please note that heaters with different dimensions were used in cell assembly (a) (OD/ID: 2.0/1.6 mm) and cell assemblies (b) and (c) (OD/ID: 2.4/1.6 mm). Temperature was monitored with a $W_{97}Re_3$-$W_{75}Re_{25}$ thermocouple (TC) whose junction was indicated by block dots.

Fig. 5 The power–temperature diagrams (a) and Arrhenius plots of electrical conductivity (b) of TiC-MgO/Al_2O_3 heaters. Also plotted in (a) is the heater resistance measured for runs 1K1892 and 1K2894. Noted that the resistance of 1K2892 is rescaled for 0.01 Ω for convenience. Experimental specifications are summarized in Table 1. Electrical conductivity was calculated from the measured total resistance by assuming electrode resistance and changes in heater dimensions are negligible during compression. The kinks as illustrated by arrows represent keeping of a constant temperature during near uniform heating. The circled data in light gray for run 1K2881 corresponds to an anomalous temperature reading associated to the melting of the heater.

Fig 6. Electron back scattered image of recovered samples of run 1K2881 (a),1K2890 (b), 1K2894 (c) and magnified image of rectangle area in 1K2894 (d). The same cell assembly (Fig. 2a) was used in run 1K2881 and 1K2890, except heater difference, i.e. TiC-Al_2O_3 (50 wt.%) heater in run 1K2881 and TiC-50 heater in run 1K2890. TiC-70 heater was used in 1K2894 with cell assembly shown in Fig. 2b.

Fig. 7 Images of cell assemblies obtained by X-ray radiography. Cell assembly with TiC-50 heater (MA41) before compression (a) and at 10.8 GPa (c) in comparison with the same cell assembly but with graphite heater, before compression (b) and at 7.4 GPa (d).

Fig. 8 Normalized CAESAR scans of liquid Fe-S alloys collected at 10.0 GPa and 1400 K using the TiC-50 heater (a) (MA41), 6.4 GPa and 1400 K using a graphite heater (b) and the averaged intensity of all two theta (c). Note that the higher pressure of the experiment using TiC-50 heater contributes partially to the observed lower diffuse scattering intensity compared with the experiment using graphite heater.

Table 1: Summary of maximal temperature generated at high pressure using the TiC heater. The prefixes "1k" and "MA" in the run numbers correspond to the 1000-ton press installed at the Institute for Planetary Materials (Okayama University), and multi-anvil press installed at the SOLEIL synchrotron facility, respectively. TiC-Al_2O_3, TiC-50 and TiC-70 refers to heaters made of TiC mixed with 50 wt.% Al_2O_3, 50 wt.% and 30 wt.% MgO, respectively. Cell a, b and c refer to assembly showed in Fig. 4. The heater size is defined by outer diameter, inner diameter, and length (in this order).

Run NO	Heater material	Cell	Heater size (mm)	P (GPa)	Highest T (K)
Heater test experiments					
1K2881	TiC- Al_2O_3	a	2.0/1.6/4.0	~ 10	1970
1K2890	TiC- 50	a			1770
1K2892	TiC- 50	b	2.4/1.6/4.0		2170
1K2894	TiC- 70	b			2250
In-situ X-ray experiments					
MA41	TiC- 50	c	2.2/1.6/3.7	10	2145
MA45	TiC- 70	c	2.2/1.6/3.7	11.5	1900
MA55	TiC- 50	c	2.4/1.8/3.5	14	2070

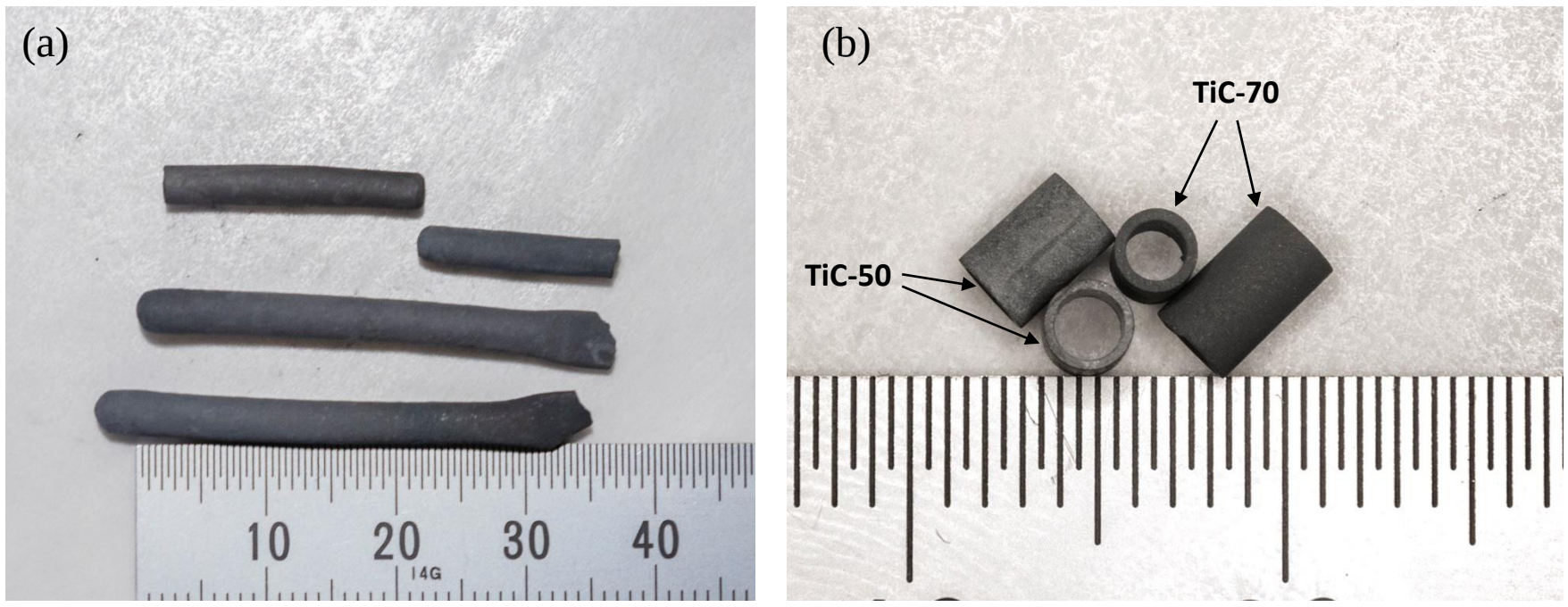

Fig.1 Pictures of synthesized TiC-MgO blocks (a) and machined tubes (b). The color difference in (b) is due to the low/high TiC (50/70 wt.%) concentration. We successfully obtained tube shape heaters of 3.5-5.0 mm length with OD/ID of 2.0-2.4/1.6 mm and 2.4/1.8 (OD: outer diameter, ID: inner diameter).

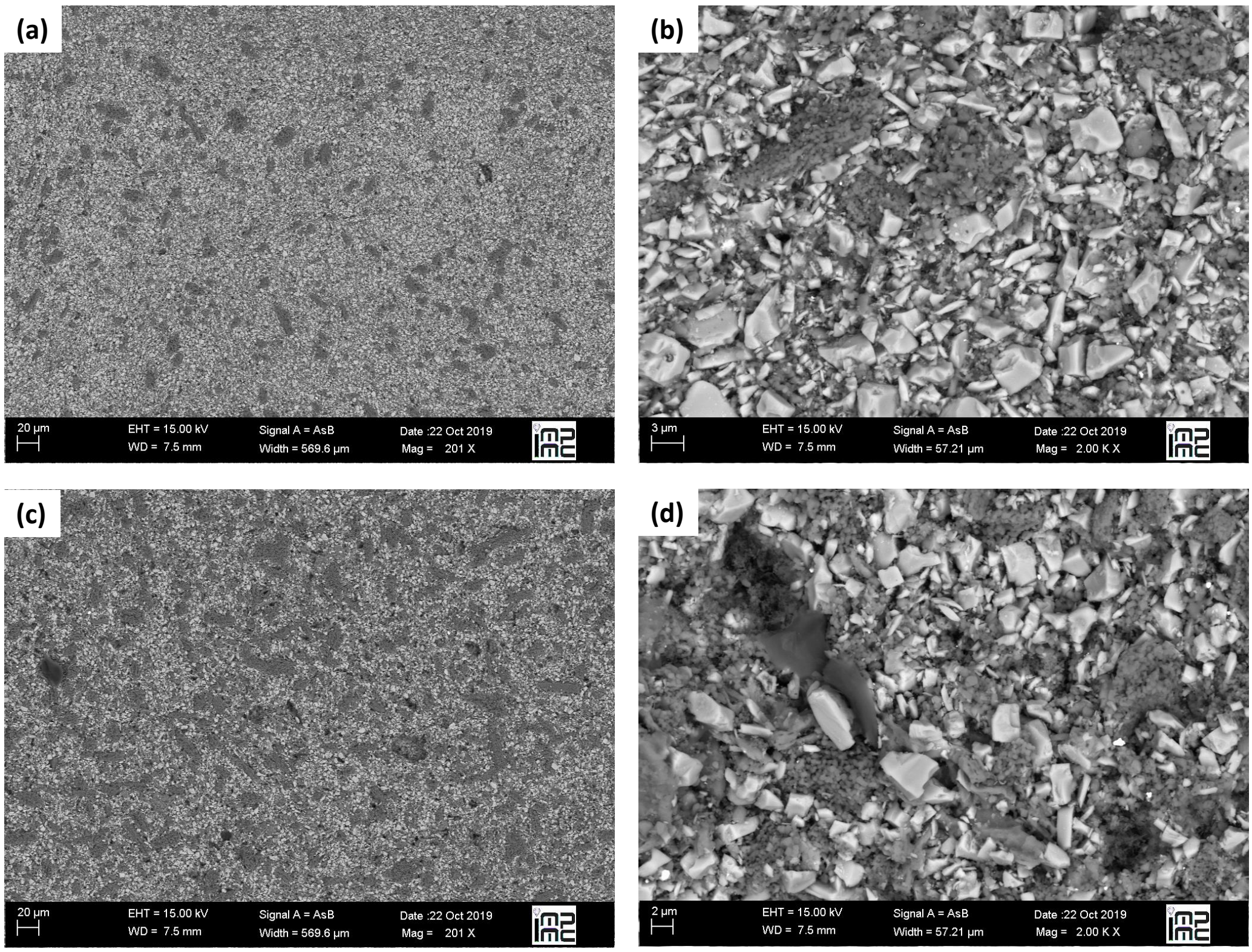

Fig.2 Electron back scattered images of sintered rods of TiC-70 (a, b) and TiC-50 (c, d). Bright and dark grains correspond to TiC and MgO, respectively.

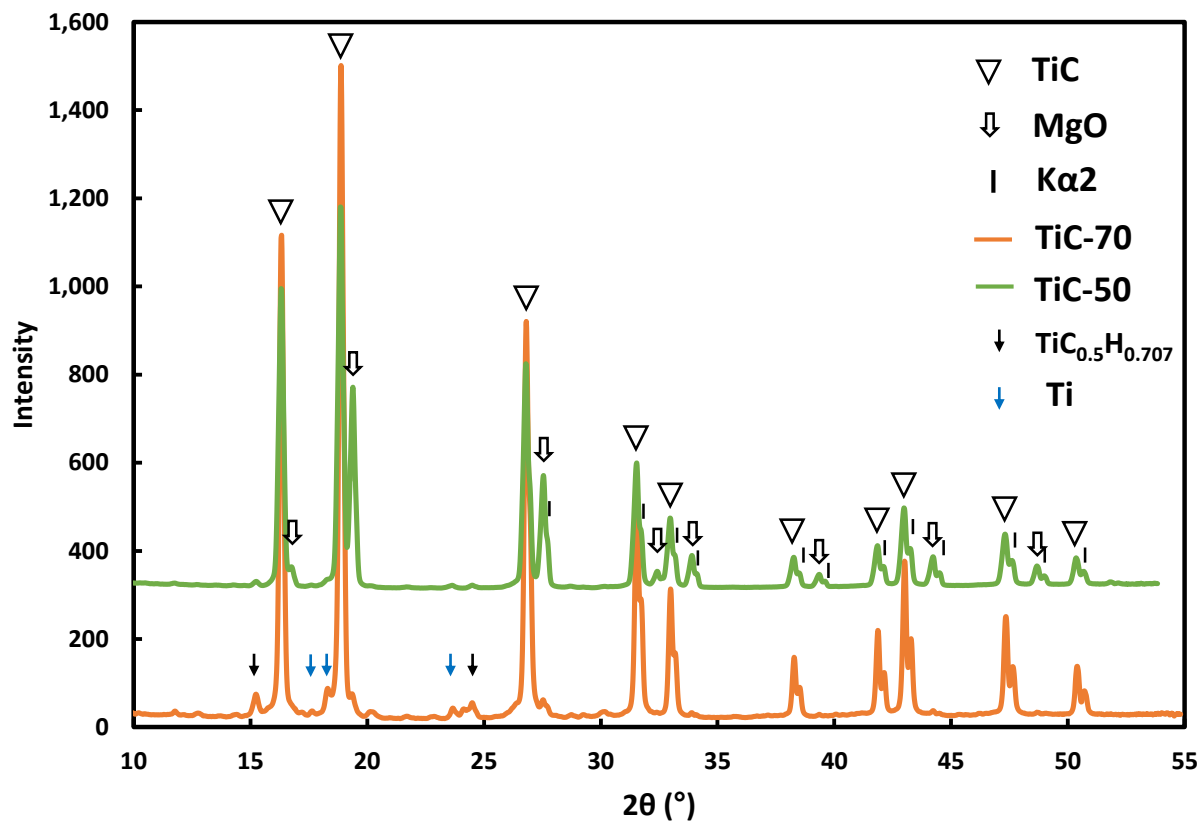

Fig. 3 X-ray diffraction patterns of the sintered TiC-MgO. Monochromatic light from a rotating Mo anode (λKα1 = 0.709319 Å) was used. The systematically observed second peaks marked by vertical sticks are diffraction peaks from Kα2 emission (λKα2 = 0.713609 Å). No obvious shift of TiC or MgO peaks was observed, suggesting no chemical reaction or inter-grain diffusion. The black arrows marked the indexed peaks of $TiC_{0.5}H_{0.707}$, by assuming same peak positions between $TiC_{0.5}H_{0.707}$ and $TiC_{0.5}D_{0.707}$.

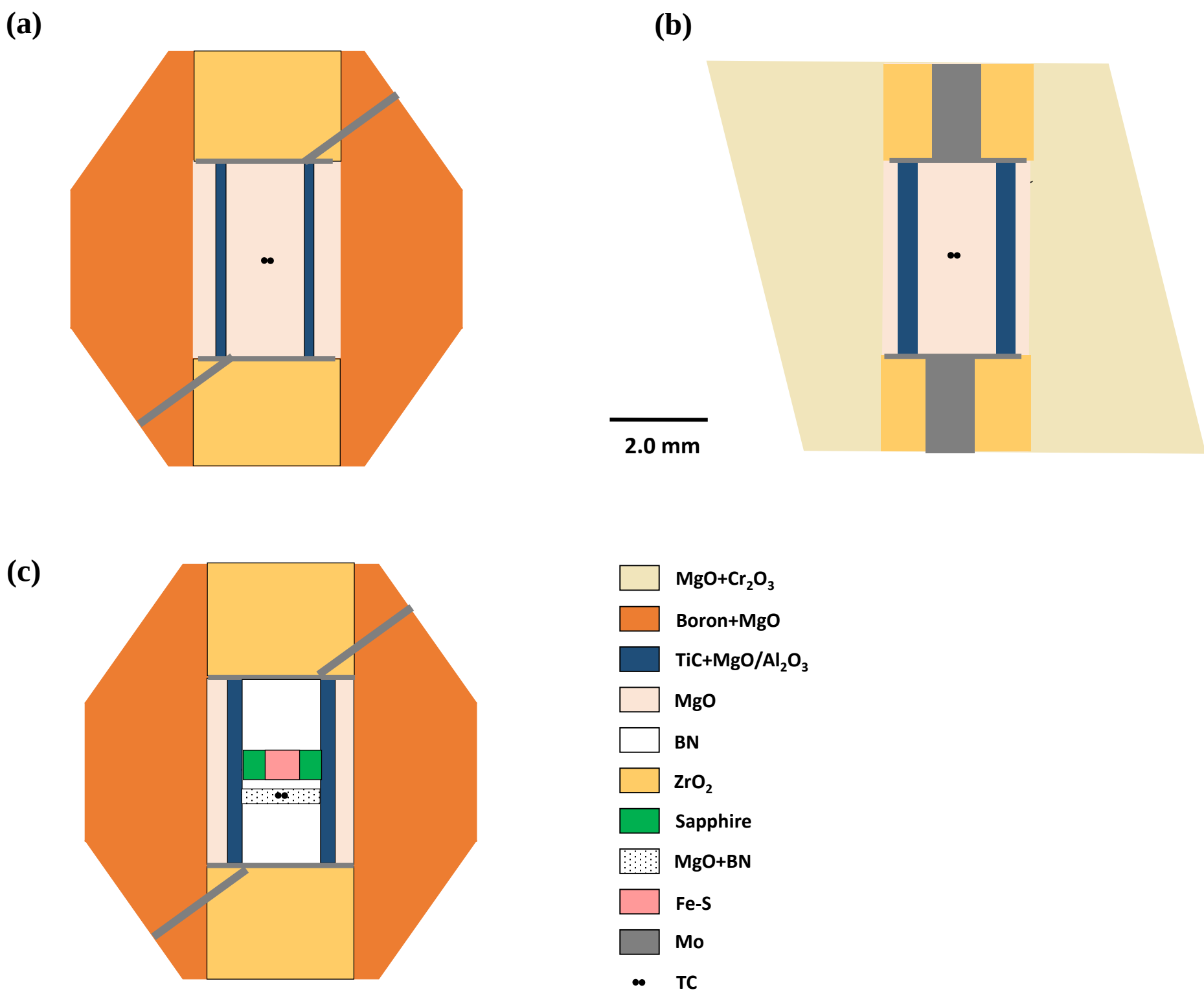

Fig. 4 Cell assemblies used for high pressure heater test experiments with boron-MgO (boron-15 wt.% MgO) (a, c) and MgO-Cr_2O_3 (MgO-5 wt.% Cr_2O_3) (b) as pressure medium. Please note that heaters with different dimensions were used in cell assembly (a) (OD/ID: 2.0/1.6 mm) and cell assemblies (b) and (c) (OD/ID: 2.4/1.6 mm). Temperature was monitored with a $W_{97}Re_3$-$W_{75}Re_{25}$ thermocouple (TC) whose junction was indicated by block dots.

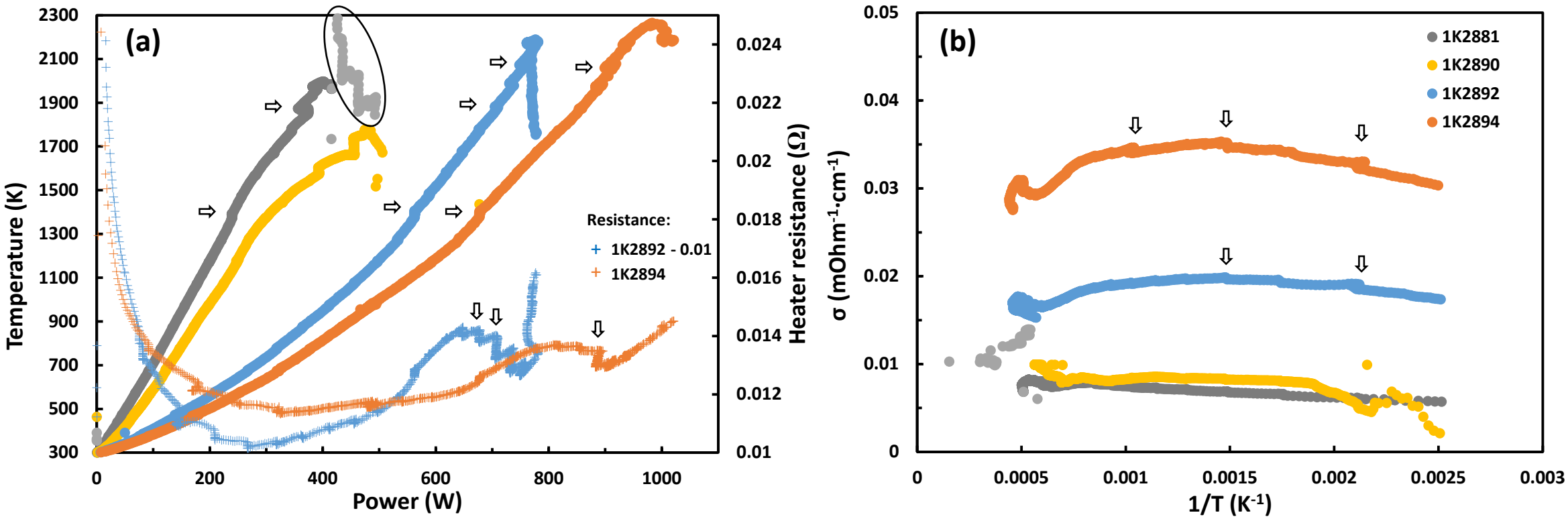

Fig. 5 The power–temperature diagrams (a) and Arrhenius plots of electrical conductivity (b) of TiC-MgO/Al_2O_3 heaters. Also plotted in (a) is the heater resistance measured for runs 1K1892 and 1K2894. Noted that the resistance of 1K2892 is rescaled by 0.01 Ω for convenience. Experimental specifications are summarized in Table 1. Electrical conductivity was calculated from the measured total resistance by assuming electrode resistance and changes in heater dimensions are negligible during compression. The kinks as illustrated by arrows represent keeping of a constant temperature during near uniform heating. The circled data in light gray for run 1K2881 corresponds to an anomalous temperature reading associated to the melting of the heater.

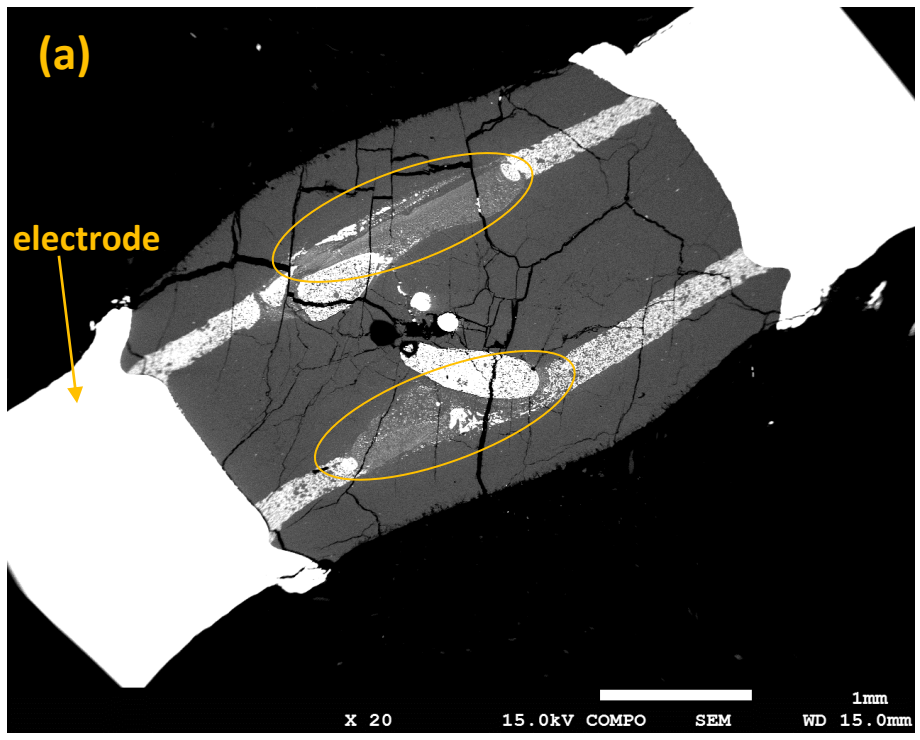

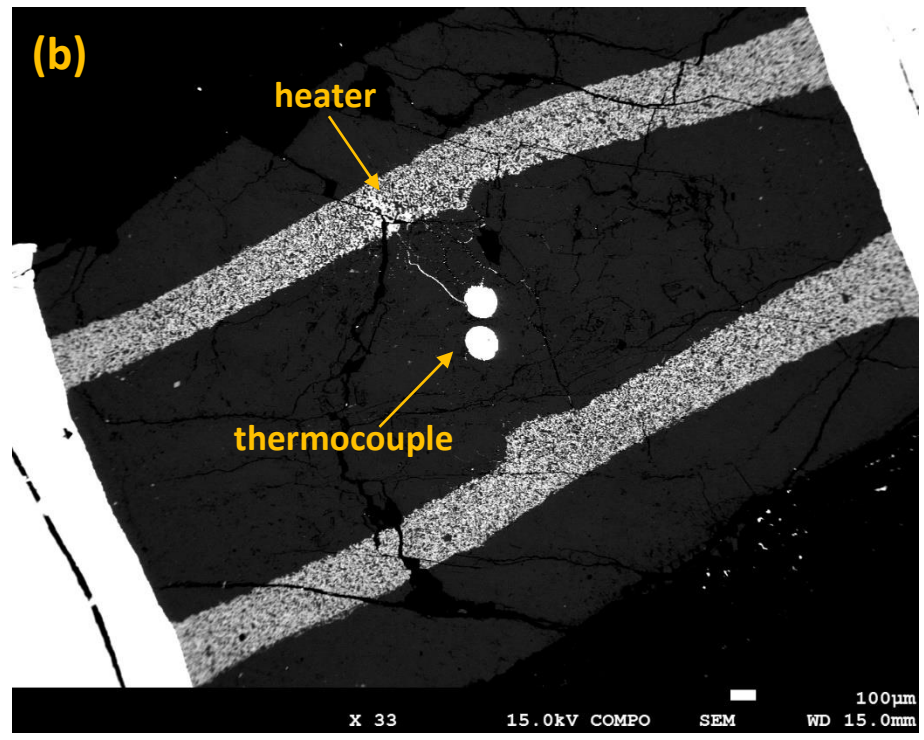

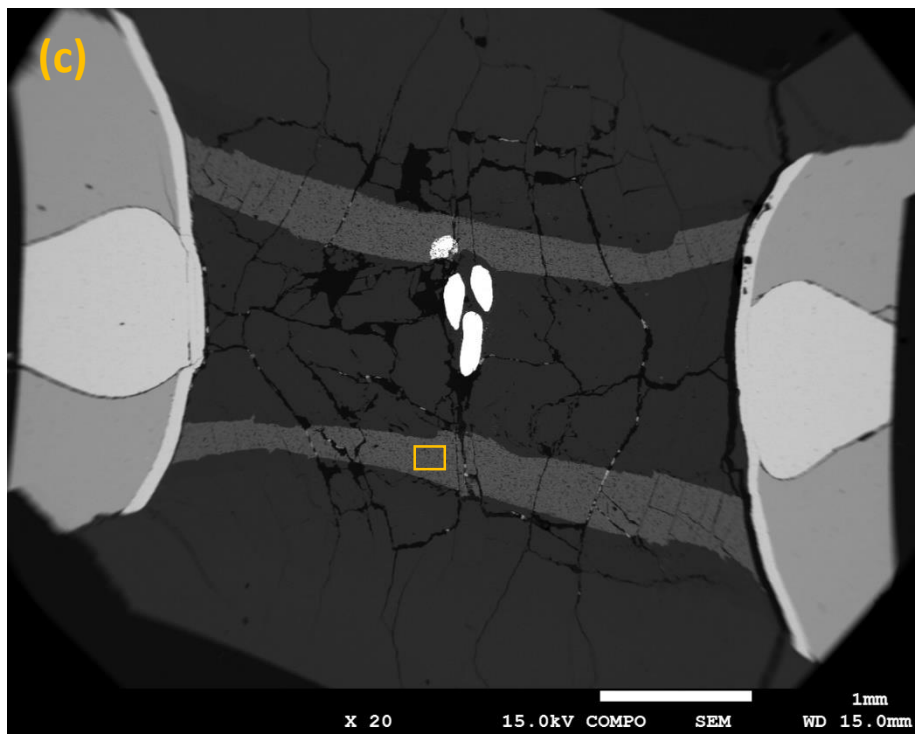

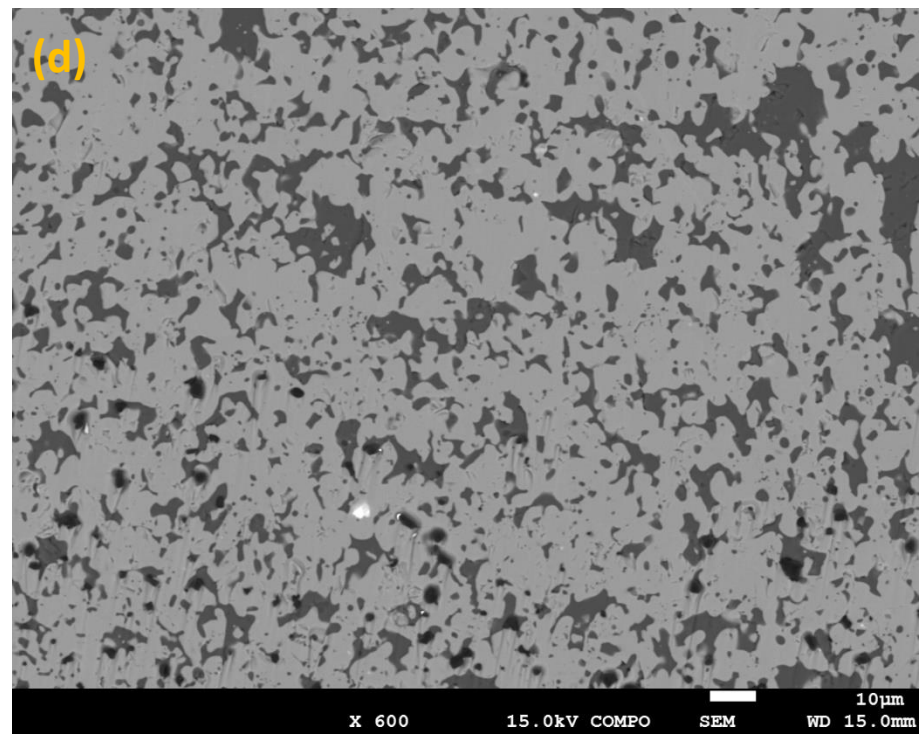

Fig 6. Electron back scattered image of recovered samples of run 1K2881 (a),1K2890 (b), 1K2894 (c) and magnified image of rectangle area in 1K2894 (d). The same cell assembly (Fig. 2a) was used in run 1K2881 and 1K2890, except heater difference, i.e. TiC-Al_2O_3 (50 wt.%) heater in run 1K2881 and TiC-50 heater in run 1K2890. TiC-70 heater was used in 1K2894 with cell assembly shown in Fig. 2b.

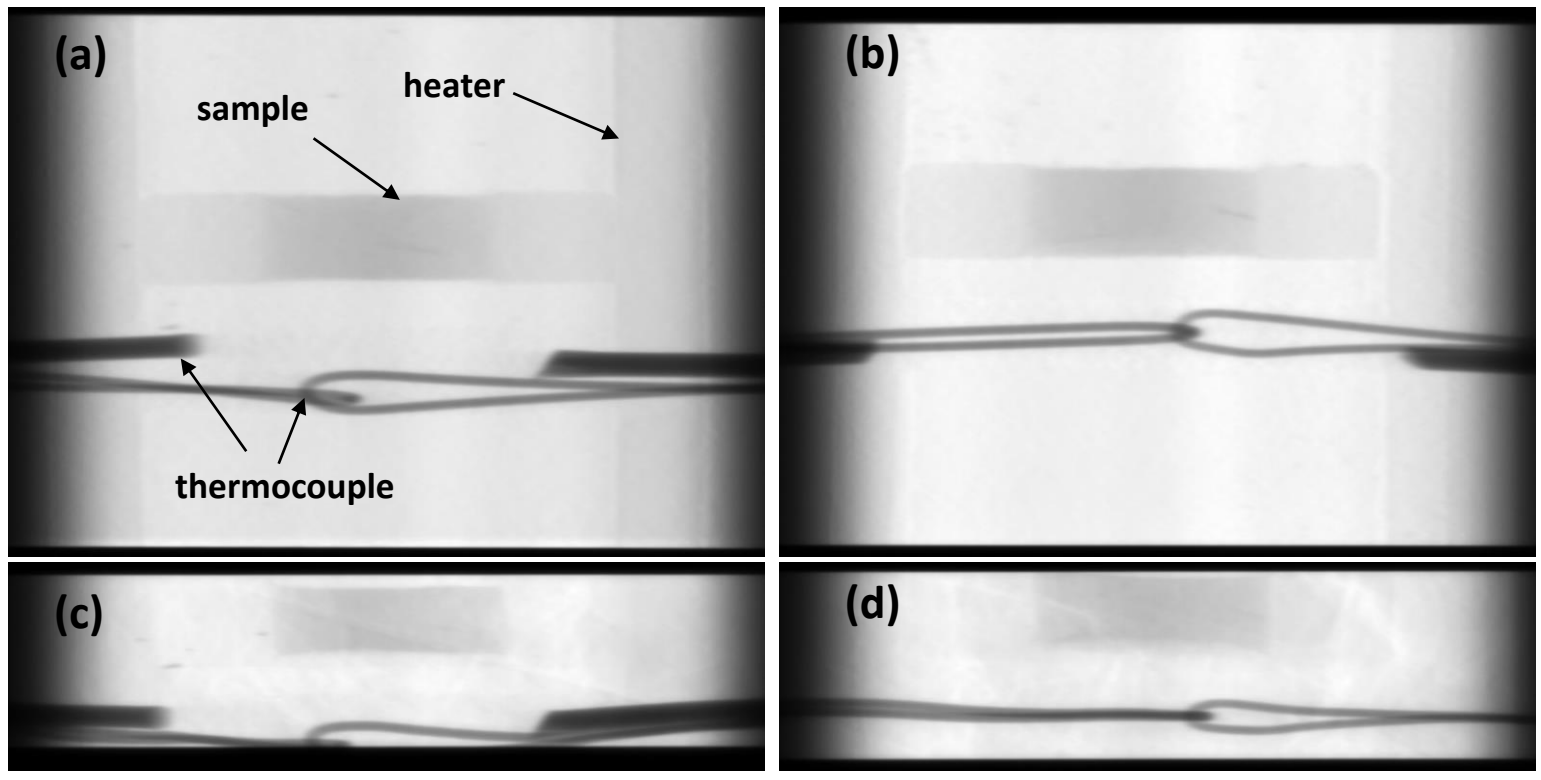

Fig. 7 Images of cell assemblies obtained by X-ray radiography. Cell assembly with TiC-50 heater (MA41) before compression (a) and at 10.8 GPa (c) in comparison with the same cell assembly but with graphite heater, before compression (b) and at 7.4 GPa (d).

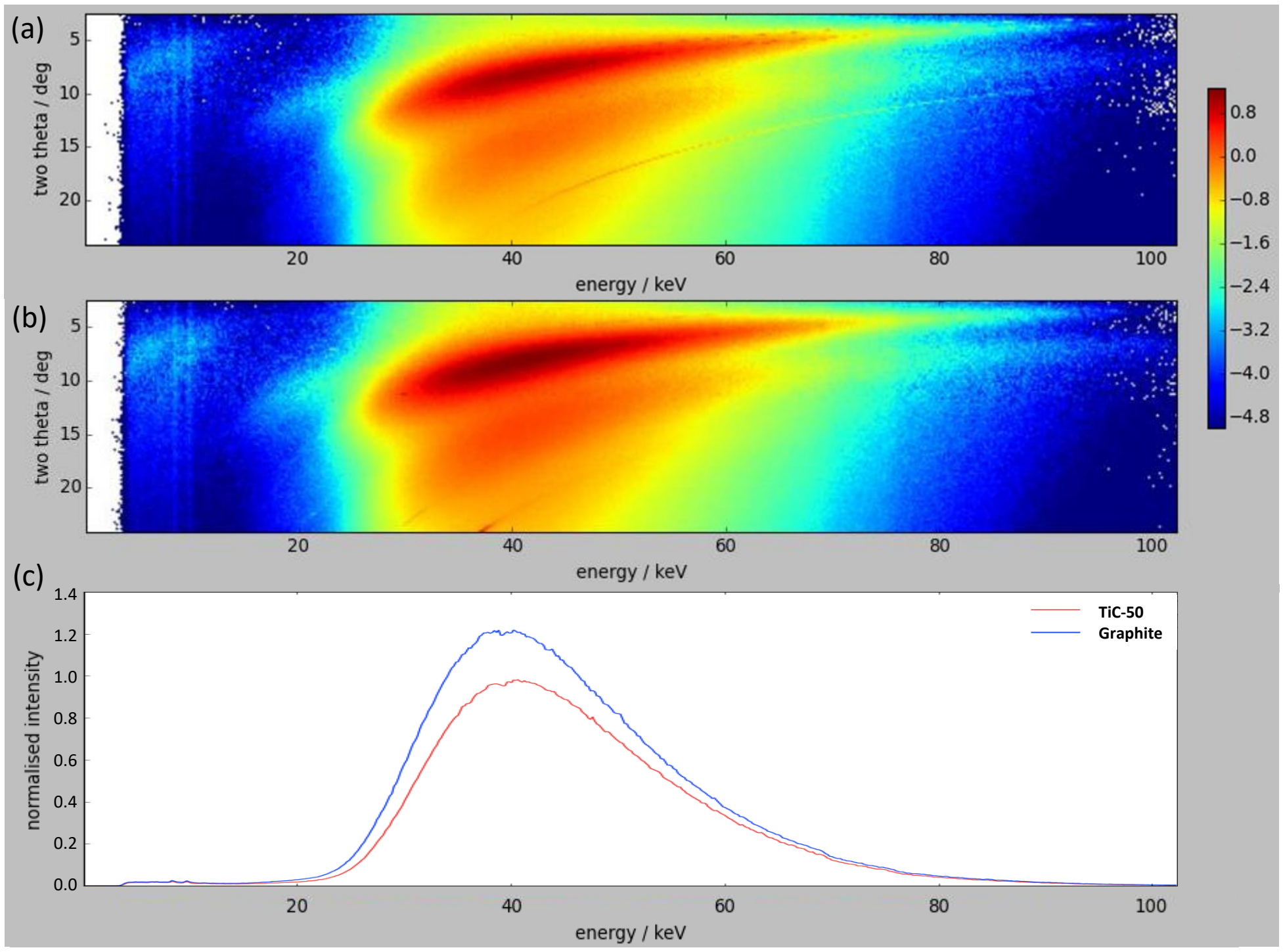

Fig. 8 Normalized CAESAR scans of liquid Fe-S alloys collected at 10.0 GPa and 1400 K using the TiC-50 heater (a) (MA41), 6.4 GPa and 1400 K using a graphite heater (b) and the averaged intensity of all two theta (c). Note that the higher pressure of the experiment using TiC-50 heater contributes partially to the observed lower diffuse scattering intensity compared with the experiment using graphite heater.